Synthesis, Structure, and Bonding of Open-Shell Sr_3In_5: An Unusual Electron Deficiency in an Indium Network, beyond the Zintl Boundary

Dong-Kyun Seo and John D. Corbett*

Contribution from Ames Laboratory−DOE[1] and Department of Chemistry, Iowa State University, Ames, Iowa 50011

Received September 18, 2000. Revised Manuscript Received March 1, 2001

Abstract: The new title compound has been synthesized and characterized by physical property measurements and electronic structure calculations. The results ratify the highly uncommon deficiency of one electron that has been long speculated for its Ca_3Ga_5-type structure on the basis of the simple Zintl electron counting formalism. In the Sr_3In_5 structure (*Cmcm*), 4- and 2-bonded indium atoms in a 4:1 ratio form a three-dimensional *classical* network that encapsulates strontium atoms in its narrow channels. The electrical conductivity of the compound shows typical *metallic* behavior. The detailed electronic structure analysis suggests that the electron hole is mainly localized on a nonbonding p-orbital on the 2-bonded indium atoms, and that these orbitals, stacked in a σ-type way along $\vec{a}$ (4.97 Å), interact only weakly with each other to form highly one-dimensional bands.

Introduction

Over recent decades, huge excitement has been brought into post-transition-metal chemistry by new discoveries that seemingly violate the Zintl rule, a well-defined relationship between the chemical structures of Zintl phases and their electronic structures according to classical octet behavior.[2−4] We and others have observed in clusters and networks newer and more complex aspects of "valence rules" that require extension of the Zintl classification to accommodate modern bonding concepts such as Wade's rules, multicenter two-electron bonding, and hypervalency. Furthermore, a significant number of post-transition and active metal compounds have been found to show *metallic* properties with *open-shell* electron configurations, although they retain other characteristics long attributed to Zintl phases, especially saltlike brittleness, stoichiometric formulations, and relatively high melting points. It is implied that phase stability can be achieved not only through covalent bonding in the anionic lattices but also via other factors such as Madelung energy and packing efficiency.[5] Thus, unusual deviations from the classical closed-shell bonding scheme may be tolerated when these other factors are equally important or even dominant in structure formation.

The simplest way of achieving a metallic character is when anionic sublattices have weak nonclassical bonds.[6] Clusters and networks of the group 13 elements (triels) are often formed via, in part, weak multicenter electron-deficient bonds. The aluminum network of $CaAl_4$ (a monoclinic variant of the $BaAl_4$-type structure) shows multicenter bond character near the Fermi level, and its metallic properties are attributed to the overlapping of the valence and conduction bands, both mainly from the anionic sublattice.[7] The relatively few cations in La_3In_5 appear to allow short intercluster contacts between closed-shell *nido*-In_5^{9-} ($2n + 4$) clusters, and therefore metallic conduction, probably because of band broadening and overlapping.[8] Cation−anion orbital interactions were found to be important for the metallic character of hypervalent $Ca_{6.2}Mg_{3.8}Sn_7$, which otherwise would be semiconducting with no band overlap.[9] In the electronic structure of $SrIn_4$ ($EuIn_4$-type; a distant cousin of the $BaAl_4$-type), the Fermi level cuts through strongly bonding and weakly bonding bands that overlap each other.[5]

Another possibility is realized among phases of extreme compositions on the active-metal-rich side with the closed-shell anionic sublattices or clusters in which excess electrons are delocalized around the cations. Studies of the lithium-rich silicides indicate that part of their structural stability comes from the formation of an additional filled state from lithium orbitals, although high in energy, which is consistent with the common fact that the character and stability of the compounds resemble those of the excessively rich element in them.[10,11] Several metallic triel cluster compounds with excess electrons have recently been found in our group, such as A_8Tr_{11},[12] $K_{18}Tl_{20}$-

(1) This research was supported by the Office of the Basis Energy Sciences, Materials Science Division, U.S. Department of Energy. The Ames Laboratory is operated for the DOE by Iowa State University under Contract No. W-7405-Eng-82.

(2) Corbett, J. D. *Angew. Chem., Int. Ed.* **2000**, *112*, 682.

(3) Kauzlarich, S. M., Ed. *Chemistry, Structure and Bonding in Zintl Phases and Ions*; VCH: New York, 1996.

(4) Nesper, R. *Angew. Chem., Int. Ed. Engl.* **1991**, *30*, 789.

(5) Seo, D.-K.; Corbett, J. D. *J. Am. Chem. Soc.* **2000**, *122*, 9621.

(6) This can be extended to some polar intermetallics with extended networks of graphite, polyacetylene, and polyacene in which bonding levels are all occupied in the (multicenter) π-bands that are continuous from most bonding to most antibonding states. See: (a) Miller, G. J. p 31 in ref 3. (b) Guloy, A. M.; Xu, Z.; Goodey, J. In *Inorganic Materials Synthesis*; Winter, C. H., Hoffman, D. M., Eds.; ACS Symp. Ser. No. 727; American Chemical Society: Washington, DC, 1999; p 2.

(7) (a) Miller, G. J.; Li, F.; Franzen, H. F. *J. Am. Chem. Soc.* **1993**, *115*, 3739. (b) Zheng, C.; Hoffmann, R. *Z. Naturforsch. B* **1986**, *41*, 292.

(8) Zhao, J.-T.; Corbett, J. D. *Inorg. Chem.* **1995**, *34*, 378.

(9) Ganguli, A. K.; Corbett, J. D.; Koeckerling, M. *J. Am. Chem. Soc.* **1998**, *120*, 1223.

(10) Nesper, R. *Prog. Solid State Chem.* **1990**, *20*, 1.

(11) Ramírez, R.; Nesper, R.; von Schnering, H. G. *J. Phys. Chem. Solids* **1987**, *48*, 51.

(12) Henning, R. W.; Corbett, J. D. *Inorg. Chem.* **1997**, *36*, 6045.

10.1021/ja0034242 CCC: $20.00
Published on Web 04/18/2001

Au_3,[13] and $K_{10}Tl_7$,[14] expanding the limit for Wade's cluster compounds.[15] The totally opposite is also feasible, as can be seen in some of the electron-rich clathrate-type tetrel compounds in which the strong classical bonds form between tetrel elements, and the outnumbered cations are isolated with cages in the tetrel lattices.[16] The excess electrons left after bond formation are eventually delocalized in conduction bands mainly composed of cationic and/or tetrel-antibonding bands.[16,17]

The most extreme situation is an open-shell configuration in a classical Zintl-like framework, i.e., one with incomplete filling of the valence bands. To our knowledge, there are eleven compounds of this kind whose reported structures should require additional electrons to have a close-shell configuration. Naked and isolated monoanions are stacked along the *c*-axis in the Fe_2P-type hexagonal structure of Mg_2In[18] and Mg_2Tl,[19] whereas isolated monoanions and dimers coexist in a 1:1 ratio in their derivatives, Mg_2Ga[19] and Li_2Sb.[20] The structures of $Ca_{11}Ga_7$[21] and $Sr_{11}In_7$[22] contain three isolated monoanions and one tetrahedron per formula unit. In the crystal structure of K_2SnBi, folded zigzag $SnBi^{2-}$ chains of alternating tin and bismuth atoms are found with a short intrachain Sn−Sn contact.[23] The anionic layers in $Ba_7Ga_4Sb_9$,[24] Li_3Al_2,[25] and $NaSn_2As_2$[26] also appear to have partially filled nonbonding orbitals. A rather strong Peierls instability was predicted in the layers in $Ba_7Ga_4Sb_9$,[27] but the structure at ambient condition does not show any distortion; however, its physical properties have not been reported for that matter. The curious Ca_3Ga_5 has a three-dimensional classical Zintl-like network containing one 2-bonded gallium as well as four 4-bonded ones in a formula unit that again is one-electron short of the closed shell.[28,29] This situation has not been explained or considered with any rigorous experimental examination. However, an unpublished ELF study showed that, of the two nonbonding states localized at the 2-bonded sites, one falls below and the other above the Fermi level.[30]

Despite their extremely unusual characteristics, however, the existence of these compounds has not been well ratified, and their importance has not been recognized in explorations of the bonding characters of intermetallics, mainly because of incomplete characterization of the compounds. During our recently initiated exploration of alkaline-earth-metal−triel systems, a new phase Sr_3In_5, isostructural with Ca_3Ga_5, was discovered. In this work, we report its structure, bonding character, and physical properties together for the first time among this class of compounds. The implications of the band properties will be discussed as well.

Experimental Section

Synthesis. Stoichiometric amounts of Sr (Alfa-Aesar, 99.9%, distilled) and In (Alfa-Aesar, 99.9995%) to give various compositions between $SrIn_2$ and Sr_5In_3 were weighed into Ta tubes in an N_2- or He-filled glovebox that had moisture levels below 0.1 ppm (volume). The tubes were arc-welded shut and then sealed in well-baked, evacuated silica jackets.[31] The vacuum system was equipped with a mercury diffusion pump, and routine work with this system was at a vacuum below discharge of the Tesla coil, i.e., $\sim 10^{-5}-10^{-6}$ Torr. The samples were first heated to 1000 °C, held for 5 h, quenched, then reheated to 760 °C, held for 5 days, and finally cooled at 10 °C/h to room temperature. The new phase was readily evident in the powder patterns of the first products, and a single crystal for structure determination was picked from a reaction loaded as Sr_2In_3. The X-ray single-crystal structure analysis showed the composition of Sr_3In_5, so this phase substitutes for the Sr_2In_3 that was tentatively assigned in previous thermal analysis studies.[32] Since thermodynamic equilibrium is obtained at the temperature used, new compositions determined by X-ray means are customarily verified by their subsequent synthesis in high yields from reactions with the indicated stoichiometries. Such a sample was first heated to 1000 °C, held for 5 h, quenched, then reheated to 600 °C, held for 8 weeks, and finally cooled radiatively to room temperature. This gave the pure phase (>95%) according to its Guinier powder pattern. There was no indication of the reaction of the samples with the Ta tubes.

The absence of hydrogen in the target compound was ensured by another set of syntheses under a dynamic high vacuum system with a cold trap cooled with liquid N_2 placed between the line and the silica tube. First, to rule out the possible existence of hydrogen in the starting materials, 400−600 mg of strontium metal was sealed in a Ta container, and this was in turn placed in a fused silica tube that was connected to the vacuum system, heated to 900 °C, held for 12 h in the dynamic vacuum, and cooled to room-temperature radiatively. The strontium exhibited a brighter luster after the treatment. The syntheses under dynamic vacuum with this purified strontium metal were done in the same way as in the static vacuum reactions. For safety reasons, however, the annealing period was shortened to 2 days at a lower temperature (500 °C). The X-ray powder pattern of the reaction product also showed the Sr_3In_5 phase in high yield (>∼70%), which proved that the Sr_3In_5 phase is not a hydride because tantalum metal at temperatures above 550 °C acts as a semipermeable membrane that allows hydrogen to pass through.[33]

Structure Determination. A shiny, silvery block-shaped crystal ca. $0.10 \times 0.09 \times 0.15$ mm^3 was mounted in a glass capillary inside the glovebox. The crystal quality was first checked with Laue photographs, and then transferred to a Rigaku AFC6R automatic diffractometer for data collection, which took place at room temperature with monochromated Mo Kα radiation. The diffraction data were corrected for Lorentz and polarization effects and for absorption with the aid of three ψ-scans of reflections with different 2θ values.

The centrosymmetric space group *Cmcm* was chosen for the structure refinement on the basis of systematic absences, the *E*-value statistics, and the Laue group indicated by SHELXTL program package.[34] A precession photograph taken for the (*hk*0) net was also in agreement with the Laue group, and no superlattice reflection was observed in it. Application of direct methods in SHELXTL revealed all of the In and Sr atoms. The full-matrix least-squares refinement converged at $R(F)$

(13) (a) Dong, Z.-C.; Corbett, J. D. *Inorg. Chem.* **1995**, *34*, 5042. (b) Dong, Z.-C.; Corbett, J. D. *Inorg. Chem.* **1996**, *35*, 2162.
(14) Kaskel, S.; Corbett, J. D. *Inorg. Chem.* **2000**, *39*, 3086.
(15) Since these compounds are in effect active-metal-rich, the gains in packing and Madelung energy are thought to be important in their stabilities.
(16) Bobev, S.; Sevov, S. C. *J. Solid State Chem.* **2000**, *153*, 92.
(17) Ramachandran, G. K.; McMillan, P. F.; Diefenbacher, J.; Gryko, J.; Dong, J.; Sankey, O. F. *Phys. Rev. B* **1999**, *60*, 12294.
(18) Schubert, K.; Gauzzi, F.; Frank, K *Z. Metallkd.* **1963**, *54*, 422.
(19) Frank, K.; Schubert, K. *J. Less-Common Met.* **1970**, *20*, 215.
(20) Müller, W. *Z. Naturforsch. B* **1977**, *32*, 357.
(21) Fornasini, M. L.; Merlo, F. *Z. Kristallogr.* **1989**, *187*, 111.
(22) Seo, D.-K.; Corbett, J. D. Unpublished results.
(23) Eisenmann, B.; Asbrand, M. *Z. Kristallogr.* **1992**, *198*, 283.
(24) Cordier, G.; Schäfer, H.; Stetler, M. *Z. Anorg. Allg. Chem.* **1986**, *534*, 137.
(25) (a) Tebbe, K.-F.; von Schnering, H. G.; Rüter, B.; Rabeneck, G. *Z. Naturforsch. B* **1973**, *28*, 600. (b) Guo, X.-Q.; Podloucky, R.; Freeman, A. J. *Phys. Rev. B* **1990**, *42*, 10912.
(26) (a) Asbrand, M.; Eisenmann, B.; Klein, J. *Z. Anorg. Allg. Chem.* **1995**, *621*, 576. (b) Eisenmann, B.; Cordier, G. p 97 in ref 3.
(27) Alemany, P.; Alvarez, S.; Hoffmann, R. *Inorg. Chem.* **1990**, *29*, 3070.
(28) Cordier, G.; Schäfer, H.; Stetler, M. *Z. Anorg. Allg. Chem.* **1986**, *539*, 33. A distortion of the Ca_3Ga_5-type structure is also found in Eu_3Ga_5 (*Cm2m* in the nonstandard setting) with a loss of the glide plane in the former space group (*Cmcm*). See: Grin, Ju. N.; Yarmolyuk, Ya. P. *J. Less-Common Met.* **1987**, *136*, 55.
(29) Although the underlying chemistry is completely different, the same structure type is also found for at least a dozen ternary compounds which have the parent structure of $Hf_3Ni_2Si_5$. See: Villars, P.; Calvert, L. D. *Pearson's Handbook of Crystallographic Data for Intermetallic Phases*, 2nd. ed.; Americal Chemical Society of Metals: Metals Park, OH, 1991.
(30) Nesper, R. Private communication, 1994.
(31) Corbett, J. D. *Inorg. Synth.* **1983**, *22*, 15.
(32) Bruzzone, G. *J. Less-Common Met.* **1966**, *11*, 249.
(33) Imoto, H.; Corbett, J. D. *Inorg. Chem.* **1981**, *20*, 145.
(34) *SHELXTL*; Bruker AXS, Inc.: Madison, WI, 1997.

Table 1. Selected Data Collection and Refinement Parameters for Sr_3In_5

space group, Z	*Cmcm* (No. 63), 4
fw	836.96
lattice parmeters (Å)[a]	$a = 4.9683(4)$, $b = 11.958(1)$, $c = 16.664(1)$
ρ_{calcd} (g cm^{-3})	5.615
μ (Mo Kα, cm^{-1})	273.73
$R1$, $wR2$[b]	0.031, 0.065

[a] Guinier powder pattern data; $\lambda = 1.540\,562$ Å. [b] $R1 = \sum||F_o| - |F_c||/\sum|F_o|$, $wR2 = [\sum w(|F_o|^2 - |F_c|^2)^2/\sum w(F_o^2)]^{1/2}$.

$= 3.1\%$, $wR_2 = 6.5\%$, and GOF $= 1.03$ for 27 variables and 825 independent reflections. The largest residual peak and hole in the ΔF map were 1.6 and -1.9 e$^-$/Å^3, respectively. Some aspects of the data collection and refinement are listed in Table 1. More detailed crystallographic information as well as the anisotropic displacement parameters are available in the Supporting Information.

Properties. Electrical resistivities were measured at 35 MHz over 110−300 K by the electrodeless "Q" method with the aid of a Hewlett-Packard 4342A Q Meter.[35] For this purpose, 74.8 mg of powdered sample with grain diameters between 150 and 250 μm was dispersed with chromatographic alumina and sealed under He in a Pyrex tube. Magnetic susceptibility measurements were carried out at 3 T over 6−350 K on a Quantum Design (MPMS) SQUID magnetometer. The powdered sample was held between the faces of two fused silica rods that were in turn fixed and sealed inside a silica tube. The data were corrected for the container and the standard diamagnetic core contributions.

EHTB Calculations. All the calculations were carried out using the CAESAR program.[36] A weighted H_{ij} formula was used for the extended Hückel calculations, and the following atomic orbital energies and exponents were employed for all the calculations (H_{ii} = orbital energy, ζ = Slater exponent): In 5s, $H_{ii} = -12.6$ eV, $\zeta = 1.903$; 5p, $H_{ii} = -6.19$ eV, $\zeta = 1.6772$;[37] Sr 5s, $H_{ii} = -6.62$ eV, $\zeta = 1.214$; 5p, $H_{ii} = -3.92$ eV, $\zeta = 1.214$.[38]

Results and Discussion

Structure and Comparisons. A ~[100] projection view of the Sr_3In_5 structure in Figure 1 shows how all atoms in the structure lie in two layers on mirror planes at $x = 0$ or $^1/_2$, and that the two layers are related by 2-fold screw axis along $\vec{c}$ (*self-duality*[39]). Three different types of indium atoms are connected together in the structure with bond distances between 2.94 and 2.99 Å; In1 is 2-bonded, and In2 and In3 are 4-bonded to other indium. Interatomic distances between strontium atoms are longer than 4.1 Å, indicating no metallic bonding between them. All of the local surroundings around In1, In2, and In3, depicted in Figure 2, have tricapped (or pseudotricapped) trigonal prismatic geometry, a common building block in many intermetallic compounds whose structures cannot be understood just in terms of close packing. Certainly, the structure formed of directly superposed atom layers must be stabilized by bond formation between the indium atoms, otherwise collapsing into an elementary closely packing structure. The environment of In1 in Figure 2 clearly exhibits a larger number of strontium neighbors than the ones around In2 and In3. As discussed later, this is consistent with the network atom that would be expected in the Zintl concept to bear the more negative charge.

A detailed description of the structure from the viewpoint of the formally In_5^{6-} network starts with the trigonal (isosceles)

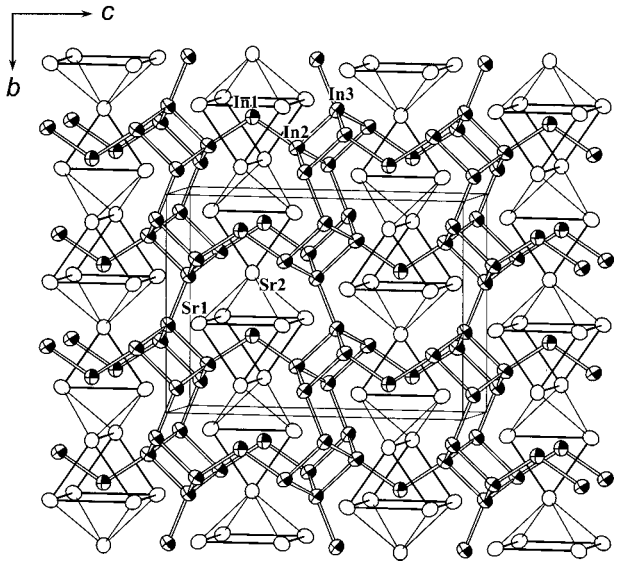

Figure 1. Off-[100] section of the orthorhombic unit cell of Sr_3In_5 down the short *a*-axis: 99% ellipsoids. All atoms lie in the same type of planes at $x = 0$ or $^1/_2$, and the planes alternate along $\vec{a}$ displaced by $b/2$ owing to a *C*-centering. The indium atoms are quarter-shaded, and the strontium atoms open. The trigonal prismatic environment around In1 is emphasized by thick lines, and the thin lines indicate Sr−Sr contacts along the channel direction.

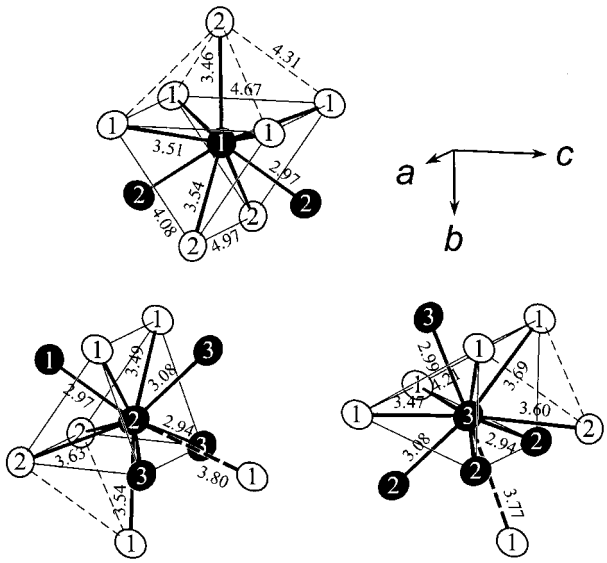

Figure 2. Environments around each of the indium atoms in Sr_3In_5. The indium atoms are solid and the strontium atoms open, and the atoms in a trigonal pyramid are connected with thin lines. All indium atoms are in tricapped (or pseudotricapped) trigonal prismatic surroundings. In1 and Sr2 have *m*2*m* symmetry.

prisms of strontium around In1 that share their triangular faces to generate an infinite structure perpendicular to Figure 1, as redrawn in a normal view in Figure 3. The trigonal prisms of atoms in the chains contain one In1 at their center, and each In1 is bonded to two neighboring In2 atoms at the same height, with a bond angle of 113.8°. Actually, each of the two In2 atoms is a part of a double zigzag chain on either side of In1, Figure 3. The double zigzag chains running along $\vec{a}$ consist of 4-bonded In2 and In3 atoms which have two nearly 90° bond angles. One bond of In3, left over after the chain formation, is used to join the chains along $\vec{b}$, Figure 1. Therefore, one might envisage the indium network in Sr_3In_5 as periodic rectangular wells; their four corners are made of indium double zigzag chains along $\vec{a}$,

(35) Zhao, J.-T.; Corbett, J. D. *Inorg. Chem.* **1995**, *34*, 378.
(36) Ren, J.; Liang, W.; Whangbo, M.-H. *CAESAR for Windows*; Prime-Color Software, Inc., North Carolina State University: Raleigh, NC, 1998.
(37) Canadell, E.; Eisenstein, O.; Rubio, J. *Organometallics* **1984**, *3*, 759.
(38) Hinze, J.; Jaffé, H. H. *J. Chem. Phys.* **1963**, *67*, 1501.
(39) O'Keeffe, M.; Hyde, B. G. *Crystal Structures−I. Patterns and Symmetry*; Mineralogical Society of America: Washington, DC, 1996; p 175.

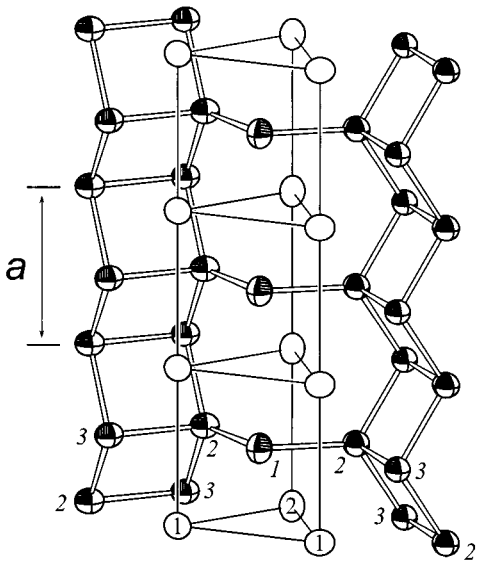

Figure 3. Two double zigzag chains of In2 and In3, and intervening 2-bonded In1 atoms. The indium atoms are quarter-shaded, and the strontium atoms open. The In1 atoms are aligned to form a one-dimensional chain along $\vec{a}$ with a repeating distance of 4.97 Å.

and they are joined perpendicularly either by direct connection (along $\vec{b}$) or through intervening 2-bonded In1 atoms (along $\vec{c}$). The strontium atoms are packed and surrounded by the rather holey walls of indium. Were the In2−In1−In2 bond angle to be much larger than 113.8°, the framework would be really open. However, the facts are that Nature abhors a vacuum, and that the close contact between the cations and anions always has to be established in stable structures. In fact, the importance of packing of cations and anions in polar intermetallics has been emphasized in our recent studies on $SrIn_4$[5] and AGa[40] (A = Ca, Y). Especially the latter compounds with the orthorhombic CrB-type structure are quite related to Sr_3In_5 in that the local environment around In1 (a tricapped trigonal prism in Figure 2) and the way of packing the prisms along $\vec{a}$ and $\vec{b}$ are exactly the same as in the CrB-type structure. The only, but big, difference is that in the CrB-type structure the "V"-shaped anionic unit (that is, the In2−In1−In2 unit in Sr_3In_5) continues and repeats along $\vec{c}$ to form single parallel zigzag chains. Further implications of this structural relationship are given in the next section.

A slightly different look can connect the indium network of the Sr_3In_5 to those of other closely related compounds. Figure 4 shows the orthorhombic structure of $BaIn_2$[41] ($CeCu_2$- or $SrAl_2$-type) in which the unit cell is oriented so that the connectivity of indium double zigzag chains to the neighbors can be easily compared with that of Sr_3In_5 in Figure 1. The differences in those two indium networks are mainly the fact that the double zigzag chains in $BaIn_2$ are now joined directly along the two perpendicular directions without any intervening atoms. The resultant channels are much narrower, and barium atoms are packed in a zigzagging way with a close Ba−Ba distance of 4.29 Å. If the structure were to be retained when barium is substituted by smaller strontium, the whole indium network must shrink. Otherwise, just maintaining close contact between indium anions and the cations, which is driven by the strong attractive forces between cations and anions, will lead to cation−cation distances in the channels much longer than what would be expected from the smaller ionic radius of strontium. However, the required shrinkage in bond distances from $BaIn_2$ seems to be too severe for the indium network to tolerate, because instead of keeping the same type of structure, $SrIn_2$ exhibits a $CaIn_2$-type "half-stuffed hexagonal diamond" structure with nearly the same average In−In bond distances as in $BaIn_2$ (3.06 Å in $SrIn_2$ vs 3.04 Å in $BaIn_2$).[41] In fact, the optimum amount of lattice compression is realized in $SrAl_2$ with much shorter anion distances,[42] and the structural parameters of this compound are surprisingly similar to those of $BaIn_2$ (Table 4), so that $SrAl_2$ is nothing more than a miniaturization of $BaIn_2$. It is noted that the strontium ions can be as close as 3.99 Å apart, as observed in $SrAl_2$. To put strontium atoms in such proximity and still keep the anion distances the same, one might change the bond angles in the indium network. However, folding the double zigzag chains in Figure 4 more severely would result in their collapse. Bringing the neighboring chains closer by changing the interchain bond angles cannot help either, eventually leading to larger channels for cations.

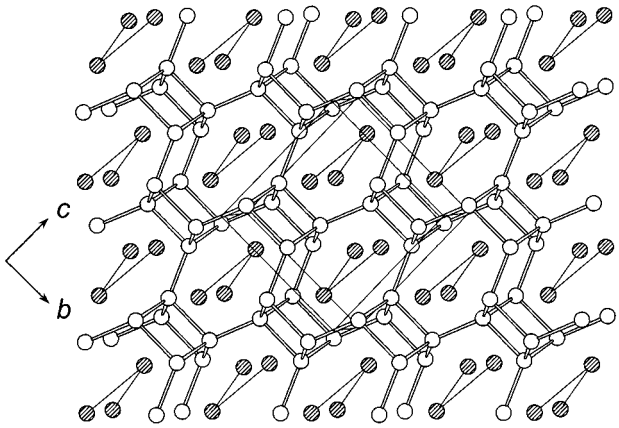

Figure 4. Off-[100] section of the orthorhombic unit cell (*Imma*) of $BaIn_2$ down the short *a*-axis. All atoms lie in the same type of planes at $x = 0$ or $^1/_2$, and the planes alternate along $\vec{a}$ displaced by $(b + c)/2$ owing to an *I*-centering. The indium atoms are open, and the strontium atoms shaded. Indium double zigzag chains are all interconnected along both $\vec{b} \pm \vec{c}$ directions. Strontium atoms zigzag along $\vec{a}$ with a contact distance of 4.29 Å which is indicated by thin lines.

Table 2. Atomic Coordinates ($\times 10^4$ Å) and Isotropic Equivalent Displacement Parameters ($\times 10^3$ Å^2) for Sr_3In_5

		x	*y*	*z*	B_{eq}[a]
In1	*m*2*m*	0	8442(1)	2500	15(1)
In2	*m*	0	2915(1)	6007(1)	14(1)
In3	*m*	0	1156(1)	4659(1)	14(1)
Sr1	*m*	0	5870(1)	8901(1)	15(1)
Sr2	*m*2*m*	0	1332(1)	2500	16(1)

[a] B_{eq} is defined as one-third of the trace of the orthogonalized U_{ij} tensor.

This problem of putting strontium atoms *in close proximity* is not solved even in the Sr_3In_5 structure; the Sr−Sr distance along the −Sr2−Sr1−Sr2− zigzag chains is 4.31 Å, which is even slightly longer than the corresponding Ba−Ba distance in $BaIn_2$ (Table 4). Interestingly as follows, this might be an unusual place where we could see an amusing trick played by the electrostatic forces that are usually thought to be dull except for providing via the Madelung energy term an additional, yet very important, stability to polar intermetallics. Let us consider the electrostatic repulsion energy between the cations only *within* each channel where the cations form a chain structure. Although the electrostatic repulsions between the cations are long-range, it is enough to consider nearest-neighbor repulsions for the discussion. In the barium zigzag chain of $BaIn_2$, each barium ion feels a repulsive energy Z^2/r from neighboring barium ions at each side, and therefore the total nearest-neighbor repulsive energy on a barium atom within a barium zigzag chain will be

Table 3. Selected Bond Distances (Å) and Bond Angles (deg) in Sr_3In_5

In1−In2[a]	2.971(1) × 2	Sr1−In3	3.470(1) × 2
In1−Sr2[a]	3.456(2)	Sr1−In2	3.489(1) × 2
In1−Sr1	3.507(1) × 4	Sr1−In1	3.507(1) × 2
In1−Sr2	3.541(1) × 2	Sr1−In2[a]	3.537(1)
		Sr1−In3	3.692(1) × 2
In2−In3	2.939(1) × 2	Sr1−In3[a]	3.775(1)
In2−In1[a]	2.971(1)	Sr1−In2[a]	3.797(1)
In2−In3[a]	3.077(1)	Sr1−Sr2	4.081(2)
In2−Sr1	3.489(1) × 2	Sr1−Sr1[a]	4.211(2)
In2−Sr1[a]	3.537(1)	Sr1−Sr2	4.307(1) × 2
In2−Sr2	3.630(1) × 2	Sr1−Sr1[a]	4.671(2)
In2−Sr1[a]	3.797(1)	Sr1−Sr1	4.968(1) × 2
In3−In2	2.939(1) × 2	Sr2−In1[a]	3.456(2)
In3−In3[a]	2.988(2)	Sr2−In1	3.541(1)
In3−In2[a]	3.077(1)	Sr2−In3[a]	3.604(1)
In3−Sr1	3.470(1) × 2	Sr2−In2	3.630(1) × 4
In3−Sr2[a]	3.604(1)	Sr2−Sr1[a]	4.081(2) × 2
In3−Sr1	3.692(1) × 2	Sr2−Sr1	4.307(1) × 4
In3−Sr1[a]	3.775(1)	Sr2−Sr2	4.968(1) × 2
In2−In1−In2[a]	113.80(5)	In2−In3−In2[b]	115.41(4)
		In2−In3−In3	119.56(2) × 2
In3−In2−In3[b]	115.41(4)	In2−In3−In2	90.96(2) × 2
In3−In2−In1	121.51(2) × 2	In3−In3−In2[a]	110.77(4)
In3−In2−In3	89.04(2) × 2		
In1−In2−In3[a]	103.77(3)	Sr2−Sr1−Sr2[b]	70.44(2)
		Sr1−Sr2−Sr1[b]	70.44(2)

[a] Bond distances and angles within the planes at $x = 0$ or $^1/_2$. [b] Bond angles of atoms zigzagging along $\vec{a}$.

Table 4. Comparison of Selected Structural Parameters (Å, deg) of Some Compounds with Parallel Double Zigzag Chains (A = alkaline-earth metal; X = triel)

	$SrAl_2$	$BaIn_2$	Ca_3Ga_5	Sr_3In_5
r_{cat}/r_{ani}[a]	1.11	1.11	1.05	1.00
$d_{X-X,av}$	2.81	3.04	2.67	2.98
$d_{A-A,chain}$	3.99	4.29	3.86	4.31
$d_{A-A,chain}/d_{X-X,av}$	1.42	1.41	1.44	1.44
$\theta_{X-X-X,zigzag}$	118.9	118.8	115.7	115.4
$\theta_{X-X-X,interchain}$	112.6	112.6	104.9	103.8
			111.2	110.8
θ_V[b]			116.8	113.8
$\theta_{A-A-A,zigzag}$	74.1	74.8	70.6	70.4

[a] Reference 5. [b] Bond angles of "V"-shaped X−X−X units (see text).

$2Z^2/r$ (where Z and r denote the charge on the cations and the nearest-neighbor distance). Compared with the $BaIn_2$ structure, the channel in Sr_3In_5 is larger and holds more strontium ions (Figure 1), which will increase the pairwise Coulombic repulsion interactions. Assuming that Sr1 and Sr2 have the same effective charge Z, the nearest-neighbor electrostatic repulsion energies on Sr1 and Sr2 will be $3Z^2/r$ ($\approx 2Z^2/r + Z^2/r'$) and $4Z^2/r$, respectively, where r and r' stand for the shortest Sr1−Sr2 and Sr1−Sr1 distances within the channels. Given the same Z and r, it is therefore clear that the cations feel more repulsion energy in the Sr_3In_5 structure than in the $BaIn_2$ structure.[43] The large electron repulsion energy among the strontium ions in the channels prevents the strontium ions from coming as close as observed in $SrAl_2$, and still allows the more distant strontium ions to buttress the indium network in Sr_3In_5.

Bonding. While $BaIn_2$ satisfies the Zintl rule with 4-bonded indium having a formal charge of −1, the classical Zintl-like indium network in Sr_3In_5 appears to be troublesome. Although the anionic structure classically requires seven electrons per formula unit from the electropositive strontium atoms ($In1^{3-} + 2 \times [In2^-] + 2 \times [In3^-] = In_5^{7-}$), the strontium atoms provide only six electrons. The one-electron deficiency presumably leads to an open valence band and affords the metallic conduction. This odd nature of the incomplete filling of the valence bands in the electronic structure of Sr_3In_5 needs a closer look. One thought from classical bonding ideas suggests that the electron deficiency should be localized around In1 atoms since they have two nonbonding orbitals that would be expected to be nearer the top of the valence band regime, and that the incomplete filling of these orbitals may not do great harm energetically.

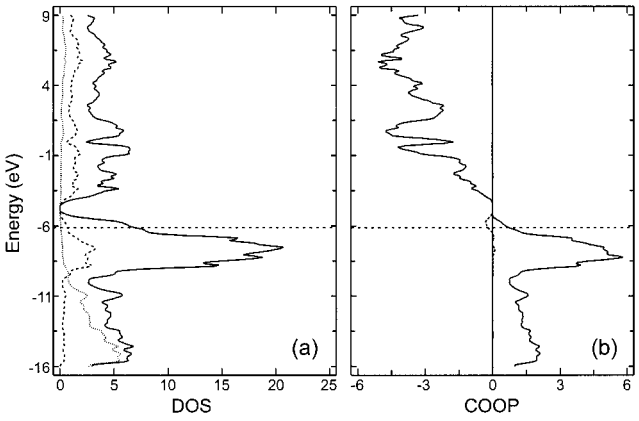

Figure 5. (a) DOS and (b) COOP plots calculated for the Sr_3In_5. In part a, the solid, dashed, and dotted lines refer to total DOS, the PDOS of Sr 5s and 5p, and the PDOS of In 5s, respectively. In part b, the solid and dashed lines represents COOP for all In−In bonds within 3.5 Å, and COOP of In1−In1 along $\vec{a}$ ($d = 4.96$ Å). The Fermi level is indicated by a horizontal dashed line.

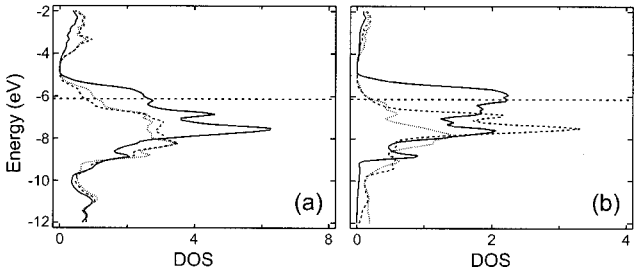

Figure 6. PDOS plots calculated for the Sr_3In_5. In part a, the solid, dashed, and dotted lines refer to the PDOS of In1, In2, and In3, respectively. In part b, the same types of lines are used for PDOS of p_x-, p_y-, and p_z-orbitals, parallel to a-, b-, and c-axes. The Fermi level is indicated by a horizontal dashed line.

The electronic band structure was calculated for the complete structure of Sr_3In_5 with the extended Hückel tight-binding method. The densities-of-states (DOS), the partial DOS (PDOS) of certain orbitals, and crystal orbital overlap populations (COOP) from the calculations are plotted in Figure 5, where the 21 valence electrons per formula unit fill the orbitals up to a Fermi energy of −6.1 eV. The Fermi level almost cuts through the top of the valence bands, mainly from indium, that are separated from the upper conduction bands by 0.6 eV, indicating a metallic behavior of the compound. With one more electron in the formula unit, the Fermi level would be brought up to the top of the valence band, and yield a semiconducting character. All this is consistent with the prediction according to the Zintl concept. The contribution of strontium below the Fermi level is small, and the calculated gross valence electron populations on Sr1 and Sr2 are 0.68 and 0.89, corresponding to +1.32 and +1.11 charges, respectively.[44]

A detailed scheme for the electronic structure of the indium sublattice can be deduced from the PDOS plots in Figure 6. Although not shown below −12 eV, the contributions from the three different indium atoms are almost the same up to −8 eV.

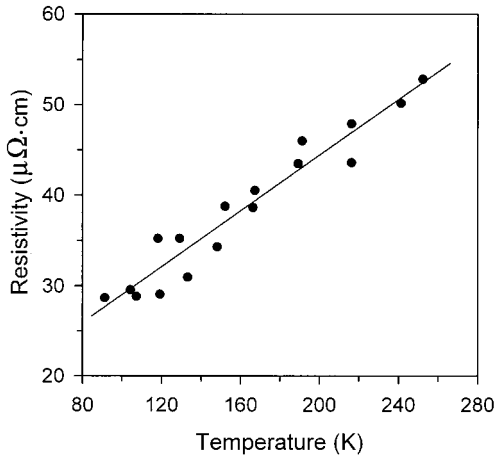

Figure 7. Temperature-dependent electrical resistivity of Sr_3In_5. Two sets of data are combined, one upon cooling and the other upon heating. No sign of hysteresis was observed. The solid line is the best fit for a linear relationship between the resistivity and temperature.

However, the dominance of In1 near the Fermi level above −8 eV in the valence band regime is made clear on a per-atom basis by the solid line in Figure 6a, which shows individual DOS contributions of the three different indium atoms. Furthermore, as can be seen in Figure 6b where the contributions of three p-orbitals of In1 are plotted separately, the crystal orbitals in this region consist primarily of highly localized p_x- and p_y-orbitals of In1 directed along $\vec{a}$ and along $\vec{b}$. Their interactions, especially of the p_x-orbitals, with neighboring In2 and In3 are very weak, close to nonbonding. Therefore, the question as to where the electron deficiency is localized is clearly answered: it is on In1, especially in its lone pair p-orbitals, as we speculated previously with the classical bonding idea. The formal charges can then be assigned as $In1^{2-}$, $In2^{-}$, and $In3^{-}$ ($In1^{2-} + 2 \times [In2^{-}] + 2 \times [In3^{-}] = In_5^{6-}$). The calculated Mulliken charges (and electron counts) on In1, In2, and In3 are −1.21 (4.21 e^-), −0.65 (3.65 e^-), and −0.63 (3.63 e^-), respectively. Were the valence bands completely filled, the values would be −1.61 (4.61 e^-), −0.71 (3.71 e^-), and −0.78 (3.78 e^-) according to the calculations.

There are features in our calculation results that the Zintl concept could not have anticipated, especially the nature of the lone pair orbitals of In1. In Figure 6b, the bands from p_x-orbitals are broader than those from p_y-orbitals, and the former is cut by the Fermi level, while the latter is rather stabilized below the Fermi level. This result indicates that the two orbitals do not behave as two classical lone pair orbitals, but that the symmetry around In1 makes the orbitals interact much differently (**1**). The p_y-orbital of In1 seems to be normal: it is doubly occupied, localized and acts as a lone pair (**2**). Since the s-orbital contribution is not large, however, the band from the lone pairs is rather broad because of interactions with neighboring indium atoms. Interestingly, the p_y-orbital points directly toward Sr2 (Figure 1), and the interaction with the empty orbitals of strontium ions will certainly be beneficial for the stabilization of the lone pair as well as of the whole structure. It is noted that the shortest contact between strontium and indium, 3.456(2) Å, in fact occurs along the p_y-direction between Sr2 and In1 (Table 3). Concerning the p_x-orbitals, the relative broadness of their bands actually arises from a "weak" additional orbital interaction between In1 orbitals across the 4.97 Å repeat distance along $\vec{a}$, which would not have been expected merely from the Zintl concept. The top of the p_x bands, which is empty, is of antibonding character in interactions between In1 atoms (Figure 5b), and the antibonding character must be from antiphase arrangement of these p_x-orbitals (**3**).

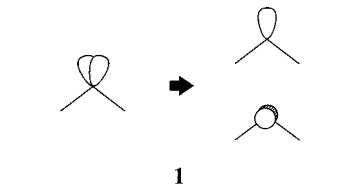

1

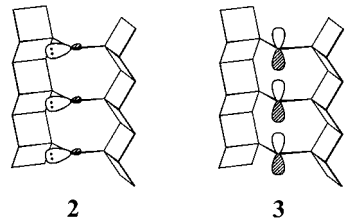

2 **3**

Although the antibonding is weak, its important role has also been noticed in understanding structural trends in the CrB-type AX (A = Ca, Sr, Ba, and Y; X = Ga, Si, Ge, Sn, and Pb) compounds, in which single zigzag chains of X atoms, in an environment exactly the same as that around In1 in Sr_3In_5, are superposed with a repeat distance of 4.19−5.29 Å.[45−47] The repeat distances are always greater than the periodic length of the chains when the X atoms have six formal valence electrons, but are shorter with five electrons. In the six-electron case, the two lone pair orbitals on each X atom are completely filled, and hence the zigzag chains become far enough apart to reduce interchain electron repulsion between π-orbitals (that is, the p_x-orbitals). When the π-orbitals are half-filled, as in the Sr_3In_5 case, the chains are closer because the top portion of the π-bands, which is antibonding, is now empty. Therefore, with the same logic, it may be argued the other way round, that the one-electron deficiency in Sr_3In_5 helps the compound retain its geometric motif of stacked In1 atoms; otherwise electron repulsion would arise between nonbonding electron pairs. However, it is still open as to whether a compound of the same structure can exist with those nonbonding orbitals fully filled.

Physical Properties. In Figure 6, the measured specific resistivities of Sr_3In_5 are seen to linearly increase from about 27 to 53 $\mu\Omega$·cm (0.36% K^{-1}) over the range of 80−260 K. The linear increase indicates that Sr_3In_5 is a normal metal in the temperature range of the measurement. This is in agreement with our previous prediction. The rather scattered data from the Q-measurements reflect the relatively large resistivity of this class of metals compared with the typical metallic elements and the corresponding small changes in *Q* values. This metallicity of Sr_3In_5 could not be seen clearly in the magnetic susceptibilties of Sr_3In_5, measured over the range of 5−360 K, because of a small amount of ferromagnetic impurities. Nevertheless, the linear paramagnetic components calculated from M vs H curves (1.0×10^{-4} and 0.7×10^{-4} emu/mol at 225 and 100 K,

(40) Zhao, J.-T.; Seo, D.-K.; Corbett, J. D. Unpublished results.
(41) Nuspl, G.; Polborn, K.; Evers, J.; Landrum, G. A.; Hoffmann, R. *Inorg. Chem.* **1996**, *35*, 6922.
(42) Cordier, G.; Czech, E.; Schäfer, H. *Z. Naturforsch. B* **1982**, *37*, 1442.
(43) The actual effective charges on the cations are expected be smaller on the Sr ions in Sr_3In_5 than on the Ba ions in $BaIn_2$ because the former ions are smaller and surrounded by the In anions with higher average formal charges. This enforces the importance of the open channel structure of Sr_3In_5.
(44) The Mulliken approximation, dividing electron pair bonding equally between the participating atoms, will, of course, make the calculated strontium charges somewhat low.
(45) Schob, O.; Parthé, E. *Acta Crystallogr.* **1965**, *19*, 214.
(46) Parthé, E. In *Structure and Bonding in Crystals*; O'Keeffe, M., Navrotsky, A., Eds.; Academic Press: New York, 1981; p 259.
(47) Fornasini, M. L. *J. Solid State Chem.* **1985**, *59*, 60.

respectively) are in agreement with the Pauli-paramagnetic behavior expected in the compound. No other singularity is observed over the entire temperature region of the measurement.

Conclusions

While numerous compounds in alkali-metal-triel systems have shown unprecedented structural and electronic diversities,[2] the same is anticipated in the scarcely explored chemistry of alkaline-earth-metal−triel systems. The divalent nature of alkaline-earth metals may mean that three-dimensional networks form more easily and frequently with more predominant triel atoms, and the role of cations—in addition to the usual space-filling and Madelung energy contributions—encapsulated in the three-dimensional covalent anionic networks can be studied. In Sr_3In_5, the interesting *active* role of the strontium atoms is that increased electrostatic repulsion energies within the channels allow the strontium atoms to buttress the indium network. In fact, the important role of cations in polar intermetallics has already been demonstrated in our recent work on $SrIn_4$, the most indium-rich compound in the Sr−In system.[5] This shows how actively the single change of active metal atoms can alter the structural formation, and even govern the structural types of the compounds in which the three-dimensional multicenter-bonded anionic network optimizes its bonding. If a ratio of cation:anion lies in the range of $0.5 \sim 1{:}1$, the cations are still outnumbered by the triels. Since the VEC (valence electron count per anionic atom) is >4 for alkaline-earth-metal-triel compounds in this composition region, *three-dimensional classical* (Zintl) networks must form with entrapped cations, as in the Sr_3In_5-type structure. The right combination of factors such as size, number, charge, and bonding character results in the existence of Sr_3In_5 despite its unusual deficiency of an octet about one indium atom. More members of this class of compounds must exist and remain to be discovered and studied.

Supporting Information Available: Tables of additional crystallographic data and anisotropic displacement parameters (PDF). This material is available free of charge via the Internet at http://pubs.acs.org.

JA0034242